Research paper

CVD-Synthesized Gallium-Oxide Thin Films as Protective Coating for Energy Storage Applications

Iqra Irfan[1], Rahul Agrawal[1], Kashif Mushtaq[1]* and Breogán Pato-Doldán[1]

[1] Department of Thermal Energy Storage, Iberian Centre for Research in Energy Storage, Caceres, 10003, Spain

***** *Corresponding author:* kashif.mushtaq@ciiae.org

Abstract: The rapid growth of renewable energy integration, particularly Concentrated Solar Power (CSP), has increased demand for reliable and efficient thermal energy storage (TES) systems. Unlike photovoltaics, CSP can provide dispatchable electricity using molten salt, typically an eutectic $Nano_3$–KNO_3 mixture, due to its broad operating range (200–600 °C), low cost, and scalability. However, long-term operation leads to corrosion and degradation of structural alloys such as stainless steels, reducing component lifespan and increasing maintenance costs. Protective coating materials with high chemical and thermal stability are therefore essential for material compatibility and TES durability. Gallium oxide (Ga_2O_3) emerged as an interesting candidate because of its wide band gap ranging from 4.8 to 5.3 eV, high breakdown field *ca.* 8 $MVcm^{-1}$, offering exceptional thermal and chemical stability, even at elevated temperature *ca.* 1800 °C, which can offer durable, effective, and efficient heat-resistant materials for TES applications. In this presented work, thin films of Ga_2O_3 are synthesized with an apparent roughness of ~1.8 nm as determined from AFM step-height profiles (mean of five measurements; ±0.4 nm) on sapphire substrate using a simple three-zone chemical vapor deposition (CVD) system, as it is cost-effective, scalable, and produces high-quality films. The preheating strategy strongly influenced surface roughness, with moderate preheating (500 °C) yielding smoother films than high-temperature preheating (750 °C). CVD enables precise control of film thickness, crystallinity, and microstructure, underscoring its potential to produce Ga_2O_3 barrier layers that resist molten-salt infiltration and thermal stress. The study provides a controlled growth process and microstructural optimization of Ga_2O_3 films, which will serve as a basis for future corrosion studies and durability testing of functional performance, which are part of the ongoing research. It is also focused on single- and multilayer architectures and protective overlayers to further enhance the corrosion resistance and interfacial stability of TES systems under harsh molten-salt cycling.

Keyword: Gallium Oxide; Chemical vapor deposition; Thermal Energy Storage System; Coating Materials

1. Introduction

The rapid development of renewable energy integration into power systems has created a huge demand for effective and reliable thermal energy storage (TES) technologies, particularly for Concentrated Solar Power (CSP) plants. In contrast to intermittent photovoltaics, CSP can supply dispatchable power through storing the solar heat in TES systems and releasing it on demand [3]. To ensure continuous power delivery, CSP plants require storage media that can absorb large amounts of thermal energy during periods of sunlight and release it efficiently during non-solar hours. This has driven the adoption of molten salts as the preferred TES medium in CSP systems, since they combine high heat capacity with chemical stability over the operating temperature window of CSP power cycles [4].

Among the molten salts, the eutectic $NaNO_3$-KNO_3 mixture (solar salt) is the most common candidate due to its 200-600 °C high-temperature operation range, low cost, and scalability [5,6]. These properties have allowed CSP plants with molten-salt storage to operate at higher capacity factors and levelized cost of electricity similar to traditional fossil-fueled power generation.

Despite their advantages, molten salts have compatibility issues with materials. Containment vessels, pipes, and heat exchangers in TES equipment are typically fabricated from stainless steels or nickel alloys, which are prone to corrosion, pitting, and microstructure degradation after prolonged exposure to high-temperature molten salts [7,8].

DOI: https://doi.org/10.66173/jenmas.2026.39
Received 10 January 2026, Revised 5 March 2026, Accepted 9 March 2026, Available online 23 March 2026

Thermal cycling also leads to crack growth, oxide spallation, and phase instability, ultimately causing component lifetimes reduction and the economic viability degradation of gas turbine power plants [9] . These issues highlight the urgent need for a reliable protective barrier coating that reduces interfacial reaction and maintains the long-term integrity of TES containers.

In this regard, the development of a stable protective coating layer becomes both a necessity for corrosion protection and system efficiency as well as minimizing maintenance costs. This motivation serves as the basis for exploring advanced oxides such as Ga_2O_3 as protective coatings for TES systems, where stability at elevated temperatures, chemical resistance, and film uniformity are requirements. The Ga_2O_3 coatings are proposed as a barrier, inhibiting direct metal-salt contact and reducing corrosion.

The rapid expansion of renewable energy integration into modern power systems has created a strong demand for efficient and reliable TES technologies, particularly for high-temperature industrial applications. Among the available TES approaches, molten salt systems have emerged as a leading candidate due to their high operating temperature range, low cost, and scalability [10,11]. However, molten salts often suffer from issues such as corrosion of containment materials, thermal degradation, and phase instability during repeated cycling, which limit their long-term performance and economic viability[12]. These challenges highlight the importance of stable interface and barrier materials that can protect TES systems and extend their durability [8].

Various classes of protective materials have been investigated for TES systems. Alumina (Al_2O_3) is chemically stable; however, it is prone to spallation due to thermal expansion mismatch when used with metals [13]. Silica (SiO_2) functions effectively as a diffusion barrier at moderate temperatures, but its performance deteriorates at higher temperatures as it softens or devitrifies above 900 °C[14,15]. Yttria-stabilized zirconia (YSZ) exhibits excellent thermal stability under high-temperature conditions, though it is costly and poses challenges in achieving uniform deposition [16,17]. Nitrides and carbides, such as silicon nitride (Si_3N_4) and titanium carbide (TiC), provide good mechanical strength but show reduced chemical stability when exposed to nitrate and nitrite melts [18]. While these materials address certain performance requirements, none offer the comprehensive combination of wide bandgap stability, mechanical robustness, and chemical inertness essential for TES environments. This limitation highlights the potential of gallium oxide (Ga_2O_3) as a next-generation barrier material for TES environments, as recent studies show stable Ohmic and Schottky contacts to β-Ga_2O_3 at elevated temperatures (up to ~400-600 °C) with long-term operation [19].

Gallium oxide (Ga_2O_3), a wide-bandgap semiconductor (4.8–5.3 eV) with a high melting point (~1800 °C), high breakdown field (8 MV/cm), outstanding thermal and chemical stability, and excellent mechanical strength, has recently attracted increasing attention [20,21]. Its unique properties make it particularly promising not only for traditional electronic and optoelectronic applications but also for emerging energy technologies[22]. In the context of TES, Ga_2O_3 offers distinct advantages as a protective thin film or barrier coating that can prevent salt infiltration, enhance corrosion resistance, and maintain the integrity of thermal storage media under harsh operating conditions [23,24]. Due to its unique properties, Ga_2O_3 is hypothesized to form a dense, stable barrier layer, reducing direct contact between the salt and metal, thereby mitigating corrosion pathways.

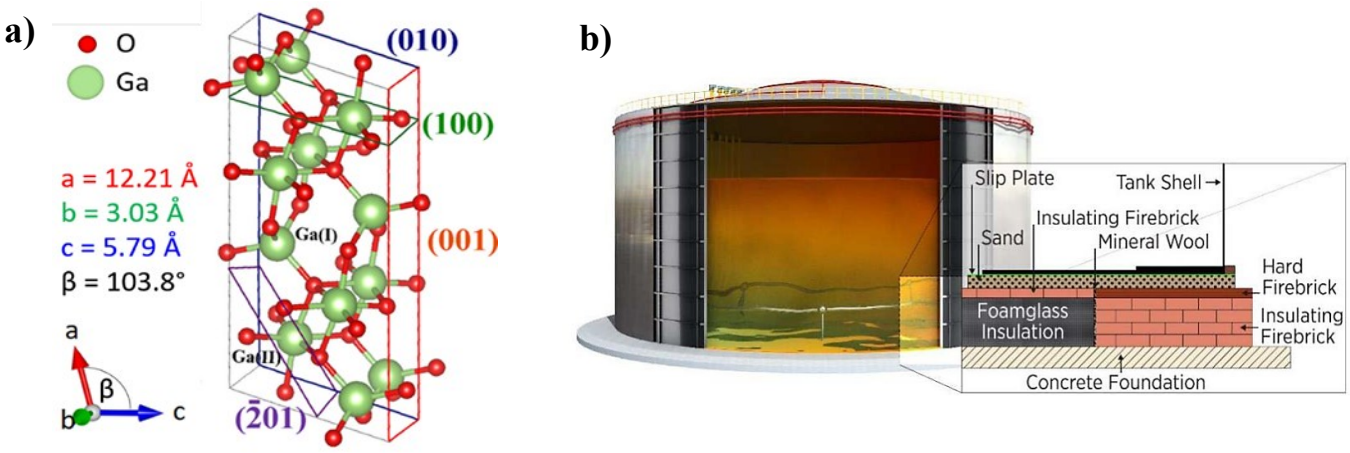

Figure 1. a) Gallium Oxide crystal structure [1] b) Container for molten salts utilized in TES systems [2]

To date, the majority of Ga_2O_3 research has been concentrated on its application in power electronics, UV photodetectors, and transparent conducting devices [25-30]. In contrast, very few studies have explored its potential in thermal management and TES systems, leaving a significant knowledge gap. In particular, understanding the growth mechanisms of Ga_2O_3 thin films and how process parameters influence their microstructure, crystallinity, and surface morphology is essential for tailoring films suitable for TES environments. Lack of systematic studies addressing how deposition parameters influence film microstructure at scales relevant to barrier applications, how microstructural features correlate with chemical stability in oxidative molten-salt environments, and the absence of clear guidelines for optimizing growth conditions to balance smoothness, crystallinity, and chemical inertness. Bridging this gap is essential to establishing Ga_2O_3 as a viable protective layer for sustainable TES systems.

A variety of deposition techniques have been employed to synthesize Ga_2O_3 thin films, including molecular beam epitaxy (MBE) [31], which yields high crystalline quality but suffers from high cost and limited scalability; metal–organic chemical vapor deposition (MOCVD), which provides precise control of composition and is widely used for device-grade Ga_2O_3 [32]; halide vapor phase epitaxy (HVPE) [33], which enables high growth rates suitable for bulk crystals; pulsed laser deposition (PLD) [34], a flexible laboratory method, though less practical for large-scale applications [35]. Chemical vapor deposition (CVD) stands out as a promising technique because of its scalability, cost-effectiveness, and compatibility with industrial processes [36]. Scalable or scalability refers to the inherent adaptability of the CVD technique, which is widely used in industrial-scale manufacturing industries, routinely employed in semiconductor fabrication, photovoltaic module production, and protective coating industries due to its ability to produce uniform and conformal films over large areas. While MBE and PLD provide excellent precision, but they are generally limited by high operational cost, complex vacuum requirements, restricted deposition area, and lower throughput, which makes them less suitable for large area industrial applications.

CVD further allows fine-tuning of growth parameters - such as temperature, gas flow, and chamber pressure - to control microstructure and surface roughness, which directly influence the protective performance of Ga_2O_3 coatings in molten salt environments [37,38]. Despite these advantages, systematic studies linking CVD growth parameters with the structural evolution and functional stability of Ga_2O_3 remain scarce, particularly in the context of TES applications.

In this work, we present a detailed investigation of β-Ga_2O_3 thin film growth by CVD, focusing on the influence of deposition parameters on film structure, morphology, and crystallinity. A combination of SEM, EDX, AFM, Raman, and XRD analyses is used to evaluate the films. Furthermore, we discuss the implications of these findings in the context of TES applications, emphasizing the role of optimized Ga_2O_3 coatings in improving the long-term stability and efficiency of molten salt systems.

It is important to clarify that the present study focuses especially on optimizing the growth parameters of Ga_2O_3 thin film using the CVD technique, along with a detailed analysis of the structural and morphological characteristics. Direct long-term durability testing in a molten salt environment is beyond the scope of this work and is currently part of our ongoing research project. The objective here is to establish control growth conditions necessary for obtaining high-quality and continuous Ga_2O_3 thin films suitable for potential high-temperature protective applications, and the findings reported here provide the necessary foundation for the subsequent corrosion, high temperature stability, and future scale-up studies.

2. Experimental

2.1 Substrate Preparation

Single-crystal sapphire (Al_2O_3, (0001) orientation, 2-inch diameter) substrates purchased from Sigma Aldrich were used for the deposition of Ga_2O_3 thin films. Sapphire substrates were selected to enable systematic optimization of growth conditions and under controlled laboratory conditions to ensure high thermal stability during deposition. Sapphire provides high thermal stability and chemical compatibility, allowing precise evaluation of temperature-dependent growth behavior. Additionally, Ga_2O_3 thin film grown on sapphire can be detached via the chemical dissolution of the substrate, allowing potential transfer to alternative substrates in future investigations. Prior to deposition, the substrates were ultrasonically cleaned in acetone and ethanol for 10 min each, rinsed with deionized water, and dried with nitrogen gas. The cleaned substrates were then placed inside the CVD chamber for film growth.

2.2 Chemical Vapor Deposition Growth of Ga_2O_3 Films

A custom-designed chemical vapor deposition (CVD) system was employed (Figure 2) in this study, enabling independent thermal control of precursor and substrate regions, facilitating optimized growth while maintaining a platform that is inherently adaptable to scale up. The deposition was carried out in a horizontal quartz tube furnace with a length of approximately 1 m and an internal diameter of 50 mm. The furnace was equipped with multiple independently controlled three heating zones, which allowed precise adjustment of the thermal profile during the preheating, transition, and growth stages. Vacuum conditions in the chamber were maintained in the range of 10^{-2}–10^{-3} mbar using a rotary pumping system, while chamber pressure was continuously monitored using a Pirani gauge and regulated through throttle valves to ensure stable growth conditions. High-purity oxygen and nitrogen gases were introduced into the chamber through calibrated mass flow controllers (MFCs) capable of delivering flow rates between 0 and 500 sccm, enabling accurate control of the oxidizing and carrier atmospheres. The gallium precursor, metallic gallium (99.999% trace metals basis, purchased from Sigma-Aldrich), was placed in an alumina crucible positioned in the upstream region of the furnace. At elevated temperatures, the gallium metal evaporated to form gallium suboxide vapors, which were transported by the nitrogen carrier gas toward the substrate region. Upon reaching the substrate, these vapors reacted with the supplied oxygen to form Ga_2O_3 films.

In the initial optimization stage, the source–substrate distance was varied between 25 and 45 cm. Based on optical microscopy, a distance of ~38–40 cm yielded the most uniform coverage (Figure 3), where the flux of reactive species and thermal gradients were optimized to promote reproducible nucleation and film growth. This optimized distance was then fixed for all subsequent experiments (Sets 1–5, Table 1). This reactor configuration provided the flexibility to systematically vary deposition parameters such as growth temperature, growth duration, oxygen and nitrogen flow rates, and preheating strategies, thereby enabling a detailed investigation of their influence on Ga_2O_3 thin film properties.

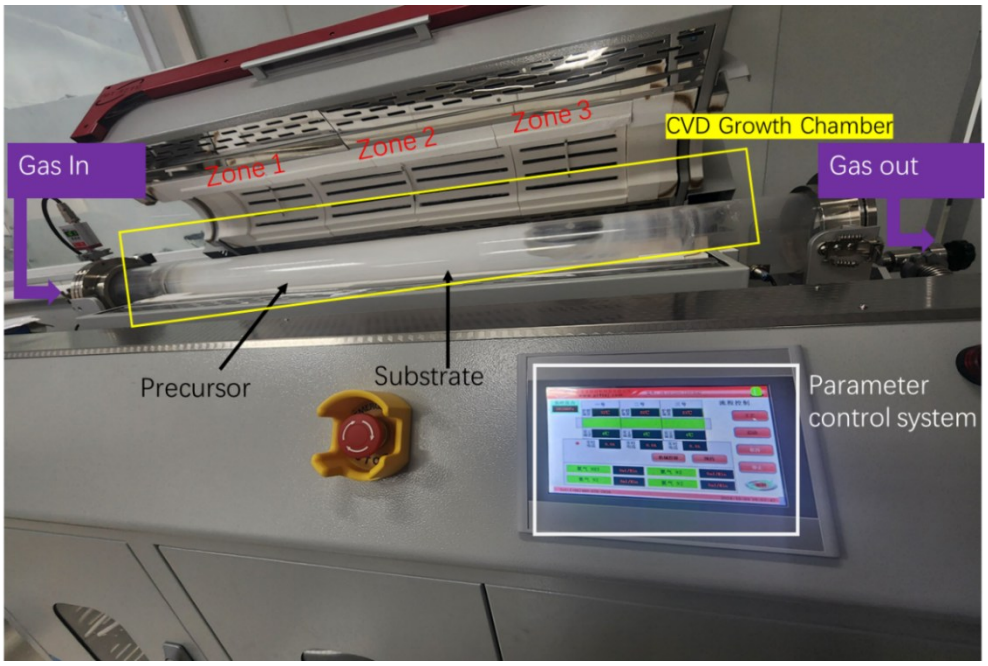

Figure 2. CVD setup with a computerized control system

2.3 Deposition Parameters

Five distinct sets of growth conditions were investigated (summarized in Table 1). These sets were designed to isolate the effect of each parameter on film properties: keeping the source-substrate distance 38-40 cm.

Table 1. Experimental conditions for Ga_2O_3 thin film growth by CVD.

Set	Preheating (°C)	Transition Temp (°C, time)	Growth Temp (°C)	Growth Time (min)	Cooling Time (min)	O_2 Flow (sccm)	N_2 Flow (sccm)
1	–	–	950	120	–	50	100
2	–	–	900	15	120	100	200
3	–	–	950	30	120	50	100
4	500	750 (20 min)	950	120	20	20	200
5	750	850 (30 min)	950	120	20	20	200

2.4 Characterization Techniques

SEM imaging was performed using a field-emission SEM setup of 360 Sigma by ZEISS operated at 10 kV accelerating voltage, working distance 8–10 mm, under high vacuum. Secondary electron (SE) and backscattered electron (BSE) detectors were used for topographic and compositional contrast, respectively. Representative images are shown for each set. Surface morphology, grain size distribution, and film continuity were analyzed. High-magnification imaging was used to resolve nucleation features, while lower magnification provided an overview of uniformity across the substrate. EDX analysis was integrated with the ZESS SEM setup to quantify elemental composition. The Ga:O ratio was monitored to assess stoichiometry under varying O_2 flow conditions. Mapping mode was used to detect local inhomogeneities (e.g., Ga-rich regions at low O_2 flow). AFM topography was acquired in tapping mode using a silicon probe with a nominal tip radius <10 nm. Scans were collected over 5 × 5 μm² and 1 × 1 μm² areas at three different locations per sample, and roughness values were averaged. Both Ra and Rq values are reported with standard deviations. 3D surface reconstructions were generated to visualize topography evolution under different preheating and flow conditions. Raman spectra were recorded by a LABRAM setup by HORIBA using a 532 nm excitation laser at 1 mW power, focused through a 50× objective lens. Each spectrum was collected with a 10 s integration time and averaged over three accumulations, with spectral resolution better than 2 cm^{-1}. Multiple locations were measured to confirm reproducibility.

3. Results and Discussion

3.1 Effect of Growth Temperature and Deposition Time

Before systematically studying the influence of CVD parameters, initial optimization was carried out to determine the effect of source and substrate distance on film formation. Optical microscopy revealed that the distance strongly influenced nucleation density and surface uniformity (Figure 2). At shorter distances, the gallium flux was too high, creating non-uniform deposits and agglomerated clusters; at longer distances, the precursor flux was insufficient, leading to sparse growth. Thus, our optimization of source–substrate distance revealed that an intermediate spacing of approximately 38–40 cm yielded the best uniformity with minimum defects. At this distance, precursor flux and thermal gradients were optimized, preventing both excessive clustering and sparse growth. This optimized spacing was therefore used for all subsequent sets of experiments reported in this study.

The influence of growth temperature and deposition time on the morphology and crystallinity of β-Ga_2O_3 thin films was further investigated. Under the optimized spacing, the baseline deposition condition (**Set 1: 950 °C, 120 min, 50 sccm O_2, 100 sccm N_2**) produced the Ga_2O_3 on the sapphire. Optical microscopy (Figure 3) confirmed largely uniform grain distribution, with isolated bright agglomerates visible in certain regions. Different morphologies are visible across the surface, including spherical particulates, irregular crystalline flakes, agglomerated clusters, and elongated whisker-like structures. This non-uniformity suggests that the chosen growth parameters promoted island growth and localized nucleation rather than layer-by-layer deposition, preventing the formation of a compact thin film. These are attributed to local supersaturation, where gallium vapor flux exceeded equilibrium growth limits. Higher-magnification micrographs (Figure 4) revealed the presence of Ga_2O_3 but with cracks and disrupted patches, which can occur due to thermal mismatch between β-Ga_2O_3 and sapphire during prolonged high-temperature deposition.

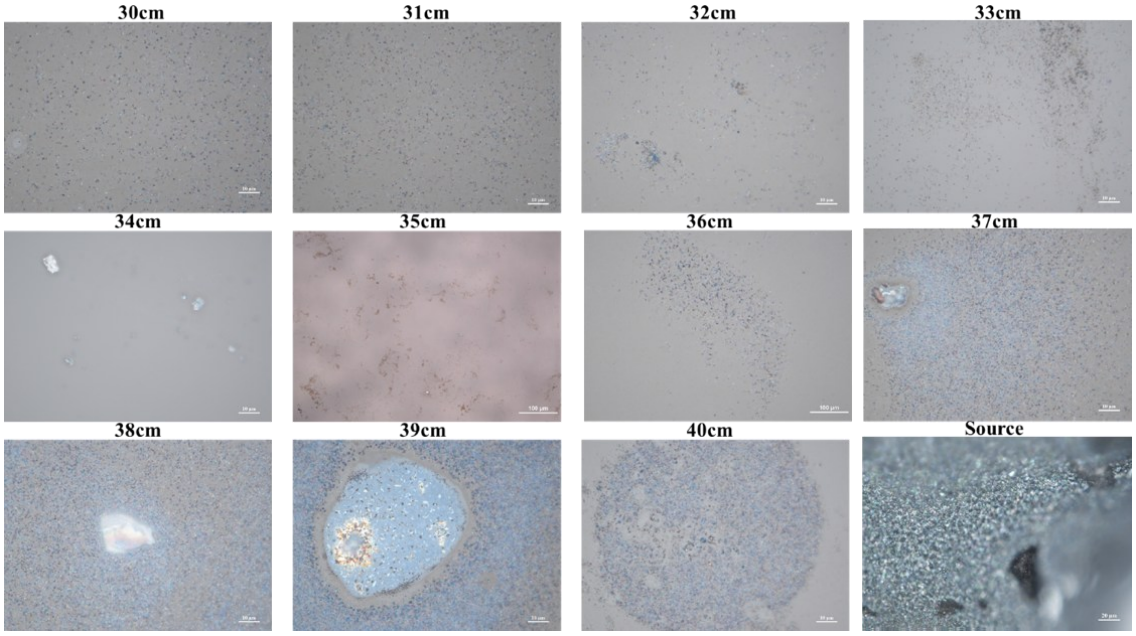

Figure 2. Optical microscopy images of Ga metal and prepared Ga_2O_3 thin films on sapphire subtrate at different source–substrate distances considering the experimental Set 1

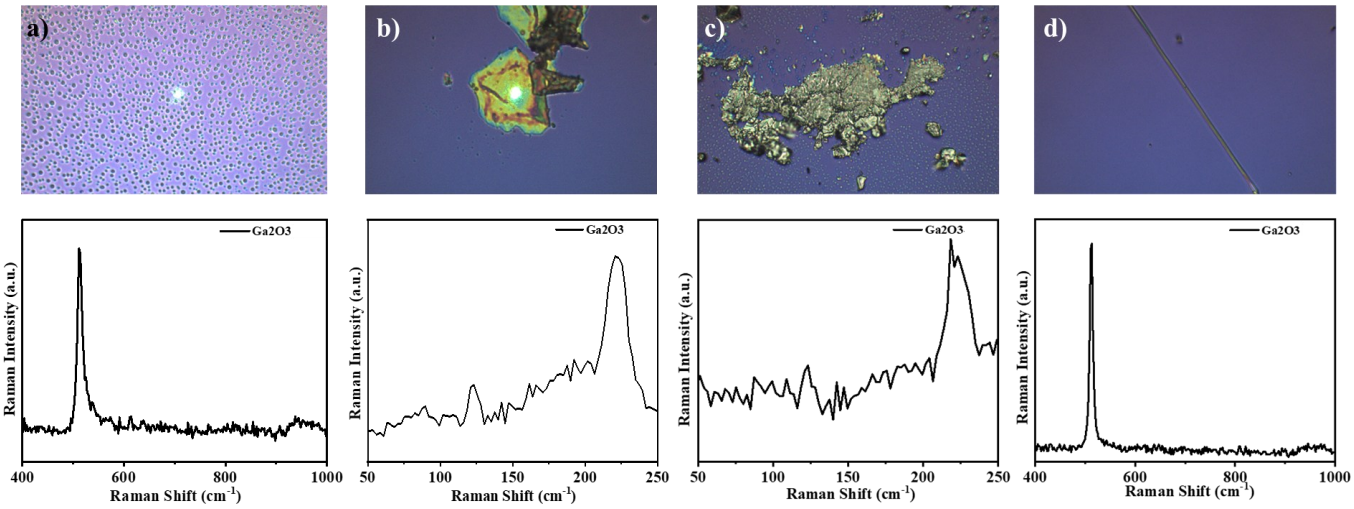

Figure 3. Optical microscopy images of as-prepared Ga_2O_3 showing different morphologies along with their Raman spectra

Raman spectra collected from these positions confirm the presence of β-Ga_2O_3 (phonon bands near ~143, 169, 199, 346, 416, 475, 633, and 767 cm. Raman spectra from Flake-like and whisker-like regions showed sharper, more intense phonon peaks, indicating higher crystallinity and larger domain sizes. In contrast, densely distributed particulates and agglomerated cluster regions showed broadened peaks, consistent with polycrystalline or partially amorphous material. Raman spectroscopy revealed gallium oxide formation at all tested growth conditions.

Together, these observations indicate that under the chosen Set 1 parameters, growth proceeds via localized nucleation and island (Volmer–Weber)-type growth, producing discrete crystalline domains rather than a continuous layer. The result suggests limited lateral coalescence arising from the combination of nucleation density [39,40], adatom surface mobility at 950 °C, and the

selected O_2/N_2 ratio that led us to parameter optimization (e.g., altered temperature, oxygen partial pressure, precursor supply, or longer growth time) to promote lateral growth and film continuity for barrier applications.

In contrast, (**Set 2: 900 °C, 15 min, cooling time 120, 100 sccm O_2, 200 sccm N_2**) when the growth temperature was set to 900 °C and the add the cooling time for 120 min, resulted in incomplete and discontinuous films. SEM images (Figure 5) revealed island-like nucleation with insufficient lateral growth to form a continuous layer. But the energy-dispersive X-ray spectroscopy (EDX) confirms the formation of Ga_2O_3. The grain size was considerably smaller, and voids remained visible between islands, indicating that the lower substrate temperature reduced the adatom diffusion length and the shorter growth time limited film coalescence. It demonstrates that both reduced thermal energy and insufficient growth time hinder the nucleation and growth process.

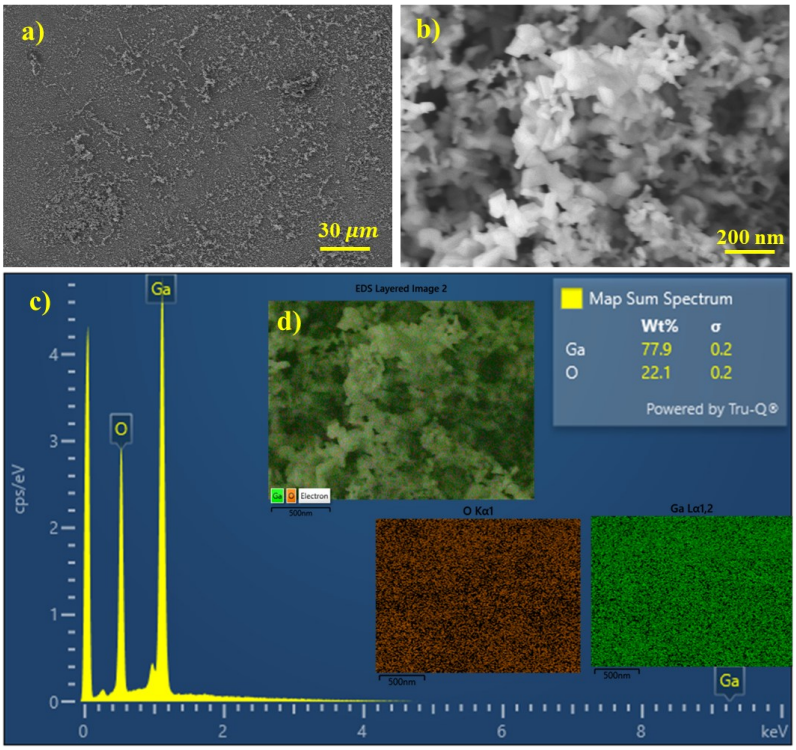

Figure 5. SEM Morphology of Set 2 at magnification a) 350 x b) 50 K x along with the c) EDX %age mapping with inset d) EDX layer image confirming the gallium oxide formation.

Based on Set 1 and Set 2, we increased the growth time from 15 min to 30 min and set the growth temperature to 950 °C. The SEM micrograph (Figure 6) showed partial coalescence, where grains were larger than in Set 2 and more bonded together. High temperature provides sufficient adatom mobility for grain growth, extended deposition time is necessary to allow full lateral coverage and defect reduction, which led us to experimental condition 4 (Set 4 as in table 1), where we use the preheating later discussed in 3.4.

These results are consistent with diffusion-limited nucleation models [41], where higher substrate temperature exponentially increases the surface diffusivity of adatoms $D_s \propto e^{-E_d/kT}$, extending their diffusion length and enabling lateral growth. Thus, dense, large-grain films form at higher temperature and longer time, a microstructural characteristic directly beneficial for thermal energy storage (TES) barrier coatings since fewer grain boundaries act as diffusion pathways for molten-salt infiltration.

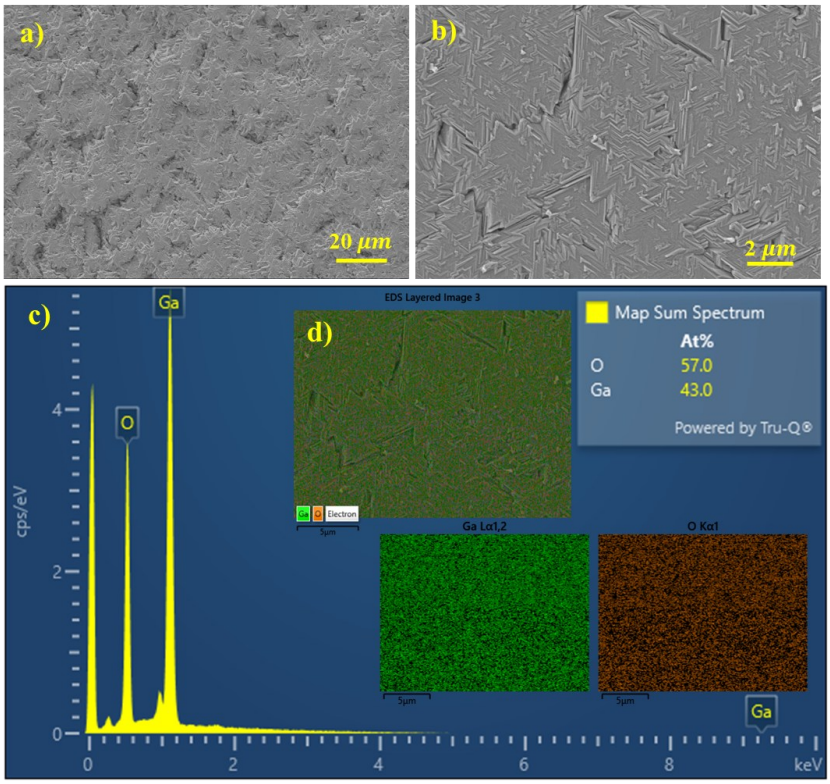

Figure 6. SEM Morphology of Set 3 at magnification a) 500 x b) 5 K x c) along with EDX %age mapping with inset d) EDX layer image confirming the gallium oxide formation.

3.2 Effect of Oxygen Flow Rate

The effect of oxygen flow rate was examined next, as oxygen partial pressure critically determines film stoichiometry and surface morphology. At a relatively high oxygen flow of 100 sccm (Set 2), EDX confirmed near-stoichiometric Ga:O composition (≈40:60, close to the ideal 2:3 ratio) as shown in Figure 5c. However, SEM images (Figure 5a) showed rough surfaces with secondary nucleation clusters, which suggests that excessive oxygen enhances surface supersaturation, leading to the formation of many small nuclei that increase roughness. When the oxygen flow was reduced to 50 sccm (Sets 3), smoother surfaces with continuous coverage were obtained (Figure 6a,b), and EDX still confirmed compositions close to stoichiometry, suggesting this as the optimal condition.

At very low oxygen flow (20 sccm, Sets 4 and 5), the SEM images (Figure 7) revealed localized gallium-rich regions, confirmed by EDX with Ga:O ratios of ≈45:55, indicative of oxygen-deficient films. Such oxygen vacancies ($V_{\ddot{O}}$) are well known to act as shallow donors in β-Ga_2O_3 [42], increasing carrier concentration but also introducing chemical instability and phonon scattering[43]. These observations can be explained in terms of nucleation thermodynamics: at very low pO_2, incomplete oxidation of gallium suboxide species yields sub-stoichiometric films, whereas at very high pO_2, the critical nucleus size is reduced due to high supersaturation, causing excessive secondary nucleation and roughness[44,45]. For TES applications, the presence of oxygen vacancies is particularly undesirable, as they serve as preferential sites for chemical attack in nitrate/nitrite molten salts. Therefore, an intermediate oxygen flow of ~50 sccm provides the best compromise between stoichiometry, smoothness, and stability.

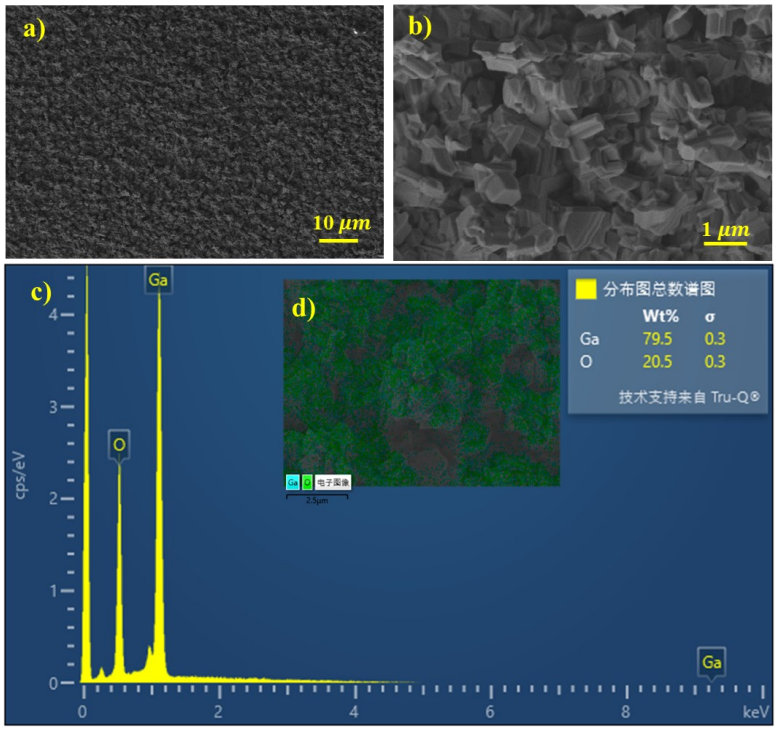

Figure 7. SEM Morphology of Set 4 at magnification a) 1 K x b) 10 K x c) along with EDX %age mapping with inset d) EDX layer image confirming the gallium oxide formation.

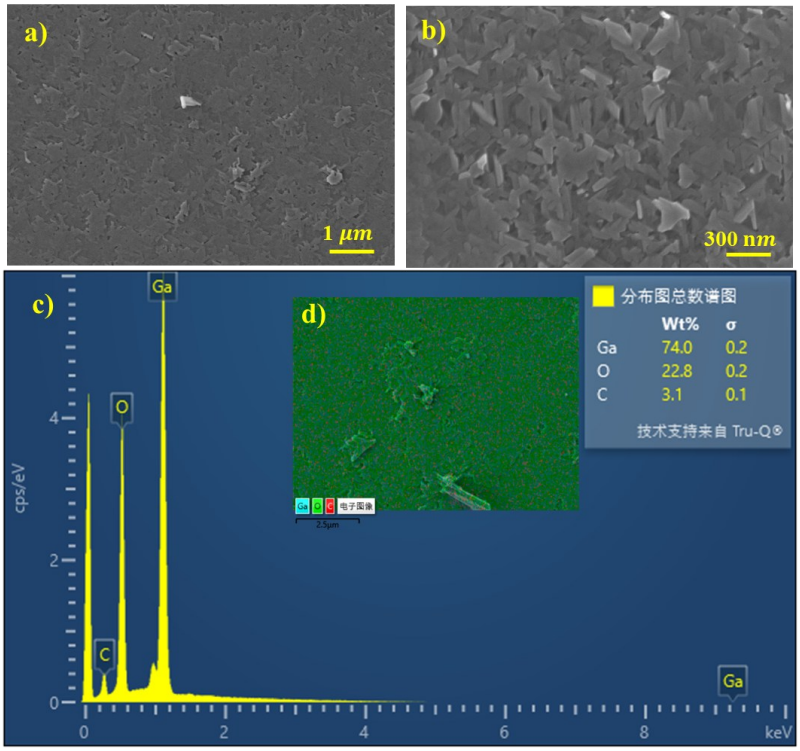

Figure 8. SEM Morphology of SET 5 at magnification a) 10 K x b) 30 K x c) along with EDX %age mapping with inset d) EDX layer image confirming the gallium oxide formation

3.3 Effect of Carrier Gas Flow

Carrier gas flow was also found to strongly influence film uniformity. Nitrogen was used as the carrier gas, and the flow rate was varied from 50 to 200 sccm to optimize the flow rate. At the higher flow of 200 sccm, the SEM images (Figure 5a) revealed uniform film thickness across the substrate, and atomic force microscopy (AFM) analysis showed root mean square roughness (≈2.5 nm, Figure 9c).

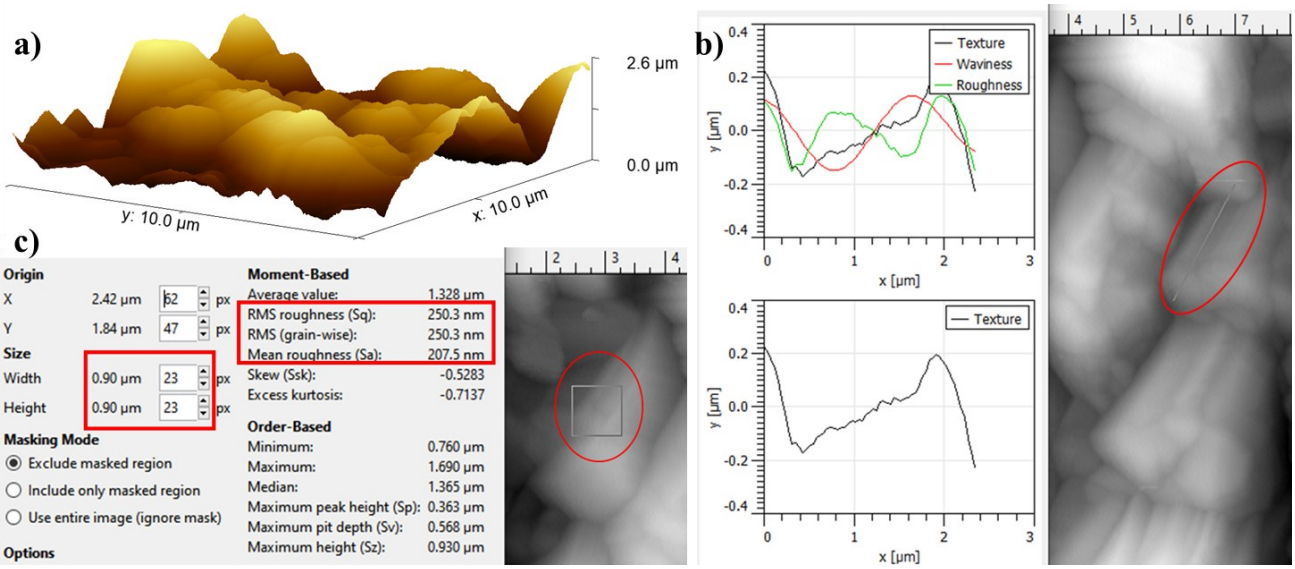

Figure 4. AFM characterization of Set2 a) 3D-surface topography b) Line roughness c) area roughness measurements.

While at the lower flow rate of 50 sccm, localized thickness gradients and still roughness were observed, as shown in Figure 10 a-c, but in parallel at this condition, we also decreased the O_2 flow rate as mentioned in section 3.1 (Figure 6a-c). For continuous formation of the film on the substrate, we optimize the combination of less O2 and higher N2 flow rates along with the preheating strategy set 4 and 5. The effect of carrier gas flow can be understood using mass transport theory [46,47]: the flux of precursors to the substrate surface is controlled by the boundary layer that develops in the gas phase. The $Sh = \frac{h_m L}{D}$ (where h_m is the mass transfer coefficient, L is the characteristic length, and D diffusion coefficient) increases with gas flow, leading to more efficient and uniform transport of reactive species[47].

At low carrier flow, precursor depletion occurs locally, resulting in uneven deposition and thickness variations.

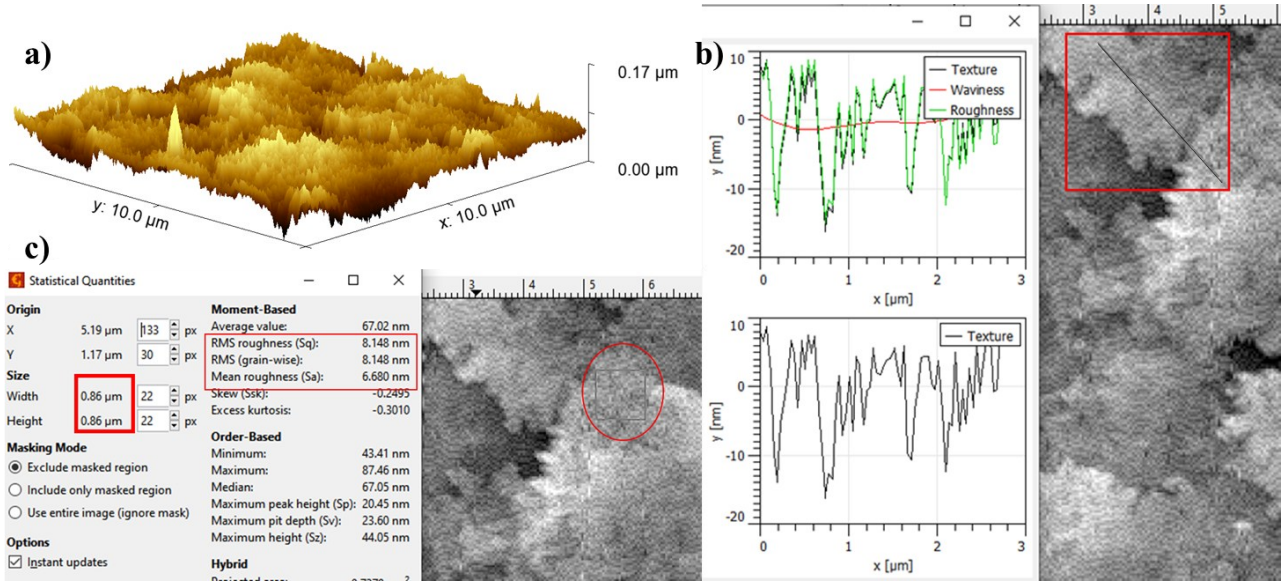

Figure 5. AFM characterization of Set3 a) 3D-surface topography b) Line roughness c) area roughness measurements.

Uniformity of barrier coatings is crucial for TES applications, as weak spots in the coating layer could allow localized molten-salt penetration, initiating corrosion pathways. Thus, higher carrier gas flows (~200 sccm) are advantageous for producing consistent films with reduced roughness.

3.4 Effect of Preheating Strategy

The preheating strategy of the substrate prior to growth had a marked effect on nucleation density and surface roughness. When the substrate was preheated at 500 °C and transitioned through 750 °C for 20 min before reaching the growth temperature of 950 °C (Set 4), SEM images (Figure 7a, b) revealed nucleation with fine grains, and AFM confirmed a low roughness of ≈1.8–2.3 nm Figure 11) as compared to Set 2 where the O_2 flow rate was high.

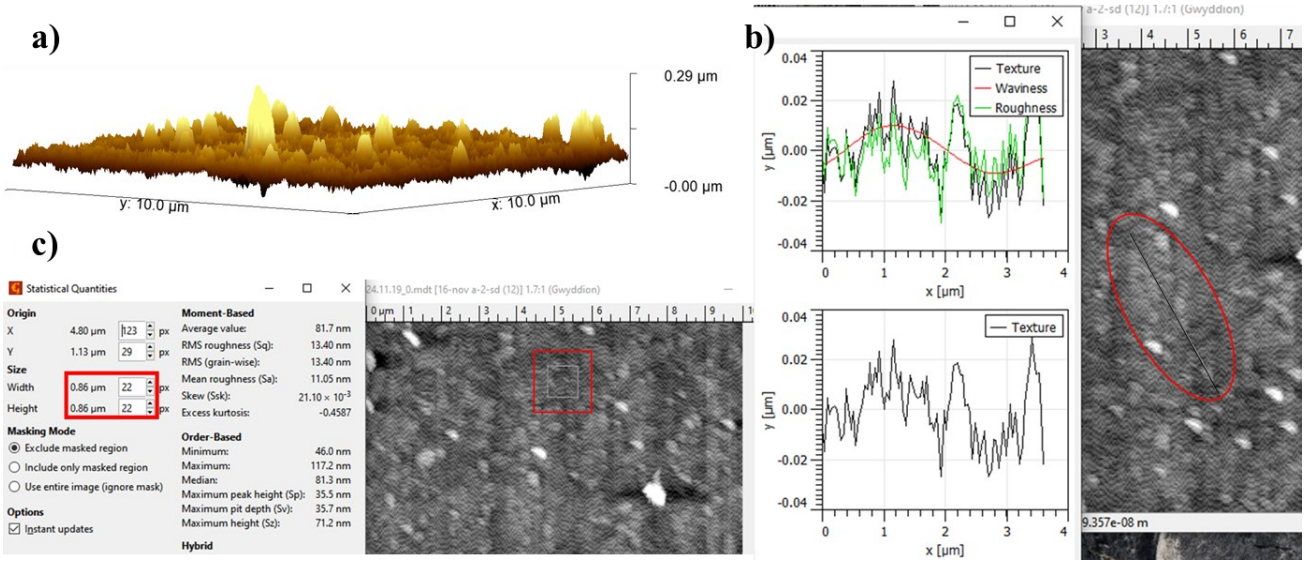

Figure 6. AFM characterization of Set4 a) 3D-surface topography b) Line roughness c) area roughness measurements.

Preheating at 750 °C with a transition stage at 850 °C for 30 min (Set 5) produced coarser, columnar grains (Figure 8) with higher roughness (Ra ≈ 4.2 nm, Figure 12). These differences can be rationalized by classical nucleation theory $N \propto exp(-\Delta G^*/kT)$ where nucleation density decreasing as supersaturation increases. At moderate preheating (500 °C), surface adsorbates such as hydroxyl groups are desorbed, cleaning the substrate and allowing high supersaturation when nucleation commences, thus producing a high density of nuclei and smoother films [45,48].

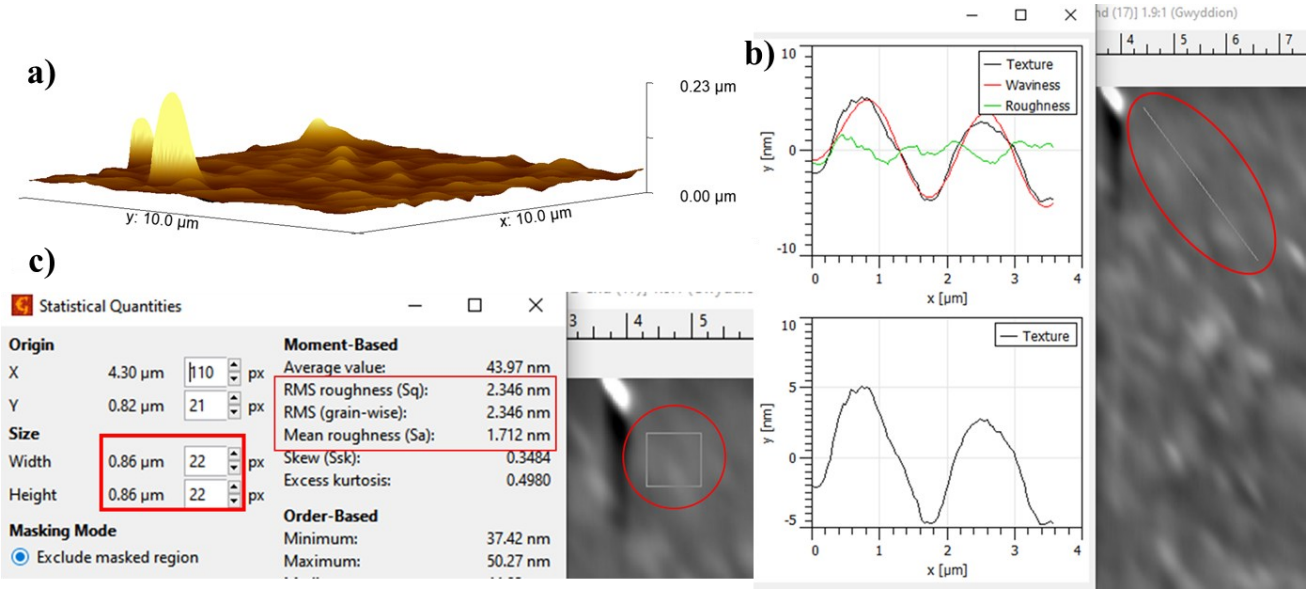

Figure 7. AFM characterization of Set5 a) 3D-surface topography b) Line roughness c) area roughness measurements.

At higher preheating (750 °C), adatom mobility is too high at the onset, reducing supersaturation and yielding fewer nuclei, which grow into larger, rougher grains via a Volmer–Weber growth mode [49].

Films grown under optimized conditions (950 °C, 120 min, 50 sccm O_2) exhibited the sharpest peaks with reduced linewidths, indicative of improved crystallinity and lower defect density. This combination was essential as it promoted adatom mobility and allowed island coalescence, resulting in a continuous, uniform film. By contrast, films grown at oxygen-deficient conditions (20 sccm O_2) exhibited broadened peaks, consistent with high oxygen-vacancy concentrations.

Table 2. Roughness of Ga_2O_3 thin film growth by CVD for each Set of experiments.

Set	Roughness
Set 1 (950 °C, 120 min)	Ra ≈ 2.3 nm
Set 2 (900 °C, 15 min)	Ra ≈ 2.50 nm
Set 3 (950 °C, 30 min)	Ra ≈ 3.5
Set 4 (preheat 500 °C)	Ra ≈ 1.8 nm
Set 5 (preheat 750 °C)	Ra ≈ 4.2 nm

4. Conclusions and Future Prospects

This study demonstrates the successful growth of β-Ga_2O_3 thin films on sapphire substrates using a custom-designed CVD system, systematically evaluating the effects of growth temperature, deposition time, oxygen and nitrogen flow rates, and preheating strategies. The consolidated results show that the optimized deposition window for Ga_2O_3 barrier coatings correspond to growth at 950 °C for 120 min, with 50 sccm O_2, 100 sccm N_2, and a preheating stage at 500 °C. Under these conditions, films exhibited smooth surface topography (Ra ≈ 1.8 nm), dense morphology, and stoichiometric composition, minimizing grain boundaries and reducing ionic diffusion pathways. These characteristics are critical for improving chemical stability and corrosion resistance when films are applied as protective barrier coatings in thermal energy storage (TES) systems.

The study further highlights that non-optimized conditions significantly compromise film quality. At lower growth temperature and shorter deposition time (Set 2), films remained discontinuous with incomplete coalescence. Excessive oxygen flow enhanced surface roughness through secondary nucleation, while insufficient oxygen introduced oxygen vacancies that reduce chemical stability. Similarly, lower carrier gas flow produced non-uniform deposition due to precursor depletion. Preheating emerged as a decisive factor: moderate preheating (500 °C) enabled desorption of surface contaminants, enhanced supersaturation at the onset of growth, and yielded smoother films (Ra ≈ 1.8 nm), whereas higher preheating (750 °C) promoted large-grain Volmer–Weber growth with higher roughness (Ra ≈ 4.2 nm).

Raman spectroscopy revealed gallium oxide formation at all tested growth conditions, but the absence of continuous films at lower temperatures or shorter times. Thus, the precise film continuity emerged only when both temperature and time reached the optimal combination (950°C for 120 min). This is a critical finding: while the reaction formed gallium oxide under all conditions, the combination of high temperature and extended time was uniquely required to achieve a uniform thin film.

Collectively, these results demonstrate that fine control over CVD growth parameters enables tailoring of Ga_2O_3 thin films with properties ideally suited for TES barrier applications. The scalability of our process is supported by the use of a three-zone CVD system that itself is inherently a scalable and practical technique. Optimized Ga_2O_3 coatings can extend the operational lifetime of TES systems by providing stable diffusion barriers against molten-salt penetration and enhancing resistance to thermal stress.

Looking ahead, two main directions for future work emerge. First, a more detailed structural validation is required, particularly XRD characterization of the deposited films, to complement Raman data and confirm phase purity. Raman confirms the formation of Ga_2O_3 vibrational modes. XRD would provide detailed information regarding crystallographic phase identification, lattice parameters, preferred orientation, and overall structural ordering of the deposited films. Such analysis would further clarify the relationship between growth parameters and crystallographic evolution of the coating. Secondly, the ongoing work establishes a single-layer coating as a foundational step towards the protective barrier development. However, a single ceramic layer may

be susceptible to stress accumulation and crack initiation during prolonged thermal cycling due to thermal expansion mismatch. To further enhance this strategy, Ga_2O_3 coatings should be integrated into multilayer architectures or hybrid protective stacks, where Ga_2O_3 can act as the primary barrier layer coupled with top layers designed to suppress crack propagation or stabilize against oxygen vacancy formation. Current efforts in our group are focused on exploring protective over-layers and multilayer stacks, which are expected to further improve corrosion resistance and interfacial stability under prolonged molten-salt cycling. This progress would move Ga_2O_3-based coatings closer to practical deployment in next-generation TES systems.

Conflict of Interest

The author declares no conflict of interest related to the publication of this research.

Data Availability Statement

The original contributions presented in this study are included in the article. Further inquiries can be directed to the corresponding authors.

Acknowledgments

This work was carried out at the laboratories of the Iberian Centre for Research in Energy Storage (CIIAE), Spain, and Shenzhen University (SZU), China.

Author Contributions

Author 1 I.I.: Conceptualization, visualization, methodology, validation, writing–original draft preparation. Author 2 R.A.: Formal Analysis, data curation, data visualization. Author 3 K.M.: Writing–review and editing, supervision, validation, resources, project administration, funding acquisition. All authors have read and agreed to the published version of the manuscript.

References

[1] Anam, B.; Gaston, N. Structural, Thermal, and Electronic Properties of Two-Dimensional Gallium Oxide (β-Ga2O3) from First-Principles Design. ChemPhysChem 2021, 22, 2362–2370. https://doi.org/10.1002/cphc.202100267

[2] Osorio, J.D.; Mehos, M.; Imponenti, L.; Kelly, B.; Price, H.; Torres-Madronero, J.; Rivera-Alvarez, A.; Nieto-Londono, C.; Ni, C.; Yu, Z. Failure Analysis for Molten Salt Thermal Energy Storage Tanks for In-Service CSP Plants; National Renewable Energy Laboratory (NREL), Golden, CO (United States): 2024. https://doi.org/10.2172/2331241

[3] D'Aguanno, B.; Karthik, M.; Grace, A.N.; Floris, A. Thermostatic properties of nitrate molten salts and their solar and eutectic mixtures. Scientific Reports 2018, 8, 10485. https://doi.org/10.1038/s41598-018-28641-1

[4] Li, N.; Wang, Y.; Liu, Q.; Peng, H. Evaluation of Thermal-Physical Properties of Novel Multicomponent Molten Nitrate Salts for Heat Transfer and Storage. Energies 2022, 15, 6591. https://doi.org/10.3390/en15186591

[5] Wang, H.; Li, J.; Zhong, Y.; Liu, X.; Wang, M. Novel Wide-Working-Temperature NaNO3-KNO3-Na2SO4 Molten Salt for Solar Thermal Energy Storage. Molecules 2024, 29, 2328. https://doi.org/10.3390/molecules29102328

[6] Kunkel, S.; Klasing, F.; Hanke, A.; Bauer, T.; Bonk, A. Concentrating solar power at higher limits: First studies on molten nitrate salts at 600 °C in a 100 kg-scale hot tank. Solar Energy Materials and Solar Cells 2023, 258, 112412. https://doi.org/10.1016/j.solmat.2023.112412

[7] Singh, M.P.; Basu, B.; Chattopadhyay, K. Probing High-Temperature Electrochemical Corrosion of 316 Stainless Steel in Molten Nitrate Salt for Concentrated Solar Power Plants. Journal of Materials Engineering and Performance 2022, 31, 4902–4908. https://doi.org/10.1007/s11665-021-06538-x

[8] Wei, Y.; La, P.; Zheng, Y.; Zhan, F.; Yu, H.; Yang, P.; Zhu, M.; Bai, Z.; Gao, Y. Review of Molten Salt Corrosion in Stainless Steels and Superalloys. Crystals 2025, 15, 237. https://doi.org/10.3390/cryst15030237

[9] Torres-Madroñero, J.L.; Osorio, J.D.; Nieto-Londoño, C.; Ordonez, J.C. Impact of molten salt inflow on the temperature distribution in thermal energy storage tanks at startup for central receiver concentrating solar power plants. Journal of Energy Storage 2025, 117, 116069. https://doi.org/10.1016/j.est.2025.116069

[10] Xiao, T.; Xu, J.; Xie, J.; Dong, X.; Liu, C.; Wang, Y.; Yu, X.; Zhang, L. Advanced encapsulation strategies for high-temperature molten salt: Synthesis methods and performance enhancement. Renewable and Sustainable Energy Reviews 2025, 218, 115818. https://doi.org/10.1016/j.rser.2025.115818

[11] Ding, W.; Bonk, A.; Bauer, T. Corrosion behavior of metallic alloys in molten chloride salts for thermal energy storage in concentrated solar power plants: A review. Frontiers of Chemical Science and Engineering 2018, 12, 564–576. https://doi.org/10.1007/s11705-018-1720-0

[12] Henríquez, M.; Reinoso-Burrows, J.C.; Pastén, R.; Soto, C.; Duran, C.; Olivares, D.; Guerreiro, L.; Cardemil, J.M.; Galleguillos Madrid, F.M.; Fuentealba, E. Long-Term Evaluation of a Ternary Mixture of Molten Salts in Solar Thermal Storage Systems: Impact on Thermophysical Properties and Corrosion. Materials 2024, 17, 4053. https://doi.org/10.3390/ma17164053

[13] Alparone, G.P.; Penney, D.; Sullivan, J.; Edy, J.; Mills, C. Al2O3 Coatings for Protection of Stainless Steel 316L against Corrosion in Zn-Al and Zn-Al-Mg. Coatings 2024, 14, 606. https://doi.org/10.3390/coatings14050606

[14] BROWN, S.D.; KISTLER, S.S. Devitrification of High-SiO2 Glasses of the System Al2O3-SiO2. Journal of the American Ceramic Society 1959, 42, 263–270. https://doi.org/10.1111/j.1151-2916.1959.tb12951.x

[15] Li, X.; Yin, X.; Zhang, L.; He, S. The devitrification kinetics of silica powder heat-treated in different conditions. Journal of Non-Crystalline Solids 2008, 354, 3254–3259. https://doi.org/10.1016/j.jnoncrysol.2008.02.016

[16] Cheng, Z.; Yang, J.; Shao, F.; Zhong, X.; Zhao, H.; Zhuang, Y.; Ni, J.; Tao, S. Thermal Stability of YSZ Coatings Deposited by Plasma Spray–Physical Vapor Deposition. Coatings 2019, 9, 464. https://doi.org/10.3390/coatings9080464

[17] Song, G.; Adamczyk, J.; Park, Y.; Toberer, E.S.; Hogan Jr., C.J. Spray Pyrolysis-Aerosol Deposition for the Production of Thick Yttria-Stabilized Zirconia Coatings. Advanced Engineering Materials 2021, 23, 2100255. https://doi.org/10.1002/adem.202100255

[18] Sato, T.; Koike, Y.; Endo, T.; Shimada, M. Corrosion and strength degradation of Si3N4 and sialons in K2CO3 and K2SO4 melts. Journal of Materials Science 1988, 23, 1405–1410. https://doi.org/10.1007/bf01154608

[19] Heinselman, K.; Walker, P.; Norman, A.; Parilla, P.; Ginley, D.; Zakutayev, A. Performance and reliability of β-Ga2O3 Schottky barrier diodes at high temperature. Journal of Vacuum Science & Technology A 2021, 39. https://doi.org/10.1116/6.0001003

[20] House, S.D.; Jiang, K.; Tang, J.; Davis, R.F.; Porter, L.M.; Das, D.; Chintalapalle V, R. Understanding Phase Stabilization and Transformations in Ga2O3 Wide-Bandgap Semiconductors Through In Situ Transmission Electron Microscopy. Microscopy and Microanalysis 2024, 30. https://doi.org/10.1093/mam/ozae044.794

[21] Sun, S.; Wang, C.; Alghamdi, S.; Zhou, H.; Hao, Y.; Zhang, J. Recent Advanced Ultra-Wide Bandgap β-Ga2O3 Material and Device Technologies. Advanced Electronic Materials 2025, 11, 2300844. https://doi.org/10.1002/aelm.202300844

[22] Zika, F.; Albagul, M.; Zhang, W.; Chodavarapu, S.; Quaglia, R.; Albagul, A. Gallium Oxide and Its Applications in Electronics: An Overview. WSEAS TRANSACTIONS ON ELECTRONICS 2024, 15, 118–127. https://doi.org/10.37394/232017.2024.15.14

[23] Song, Y.; Shoemaker, D.; Leach, J.H.; McGray, C.; Huang, H.-L.; Bhattacharyya, A.; Zhang, Y.; Gonzalez-Valle, C.U.; Hess, T.; Zhukovsky, S.; et al. Ga2O3-on-SiC Composite Wafer for Thermal Management of Ultrawide Bandgap Electronics. ACS Applied Materials & Interfaces 2021, 13, 40817–40829. https://doi.org/10.1021/acsami.1c09736

[24] Cheng, Z.; Wheeler, V.D.; Bai, T.; Shi, J.; Tadjer, M.J.; Feygelson, T.; Hobart, K.D.; Goorsky, M.S.; Graham, S. Integration of polycrystalline Ga2O3 on diamond for thermal management. Applied Physics Letters 2020, 116. https://doi.org/10.1063/1.5125637

[25] Liu, A.-C.; Hsieh, C.-H.; Langpoklakpam, C.; Singh, K.J.; Lee, W.-C.; Hsiao, Y.-K.; Horng, R.-H.; Kuo, H.-C.; Tu, C.-C. State-of-the-Art β-Ga2O3 Field-Effect Transistors for Power Electronics. ACS Omega 2022, 7, 36070–36091. https://doi.org/10.1021/acsomega.2c03345

[26] Li, B.; Wang, Y.; Luo, Z.; Xu, W.; Gong, H.; You, T.; Ou, X.; Ye, J.; Hao, Y.; Han, G. Gallium oxide (Ga2O3) heterogeneous and heterojunction power devices. Fundamental Research 2025, 5, 804–817. https://doi.org/10.1016/j.fmre.2023.10.008

[27] Pearton, S.J.; Ren, F.; Polyakov, A.Y.; Haque, A.; Labed, M.; Rim, Y.S. Status of Ga2O3 for power device and UV photodetector applications. Applied Physics Reviews 2025, 12. https://doi.org/10.1063/5.0285075

[28] Zhong, W.; Liu, Y.; Huang, H.; Sun, Z.; Xin, W.; Liu, W.; Zhao, X.; Long, S.; Xu, H. Ultrathin Ga2O3 Photodetector with Fast Response and Trajectory Tracking Capability Fabricated by Liquid Metal Oxidation. Nano Letters 2024, 24, 13769–13774. https://doi.org/10.1021/acs.nanolett.4c04030.s001

[29] Zhang, J.; Willis, J.; Yang, Z.; Lian, X.; Chen, W.; Wang, L.-S.; Xu, X.; Lee, T.-L.; Chen, L.; Scanlon, D.O.; et al. Deep UV transparent conductive oxide thin films realized through degenerately doped wide-bandgap gallium oxide. Cell Reports Physical Science 2022, 3, 100801. https://doi.org/10.1016/j.xcrp.2022.100801

[30] Zhang, K.; Feng, L.; Wang, L.; Zhu, J.; Zhang, H.; Ha, S.; Sun, J.; Liang, H.; Yang, T. Ga2O3/Ag/Ga2O3-Laminated Film Fabricated at Room Temperature: Toward Applications in Ultraviolet Transparent Highly Conductive Electrodes. Crystals 2023, 13, 1018. https://doi.org/10.3390/cryst13071018

[31] Guo, D.; Wu, Z.; Li, P.; An, Y.; Liu, H.; Guo, X.; Yan, H.; Wang, G.; Sun, C.; Li, L.; et al. Fabrication of β-Ga2O3 thin films and solar-blind photodetectors by laser MBE technology. Optical Materials Express 2014, 4, 1067–1076. https://doi.org/10.1364/ome.4.001067

[32] Sanyal, I.; Nandi, A.; Cherns, D.; Kuball, M. Thermodynamics of Ga2O3 Heteroepitaxy and Material Growth Via Metal Organic Chemical Vapor Deposition. ACS Applied Electronic Materials 2024, 6, 5021–5028. https://doi.org/10.1021/acsaelm.4c00535

[33] Kim, W.; Kim, H.W.; Cho, S.B. Design of optimized halide vapor phase epitaxy (HVPE) conditions for uniform α-Ga2O3 growth based on CFD analysis. Journal of the Korean Ceramic Society 2025. https://doi.org/10.1007/s43207-025-00523-z

[34] Sanchez, F.; Das, D.; Episcopo, N.; Manciu, F.S.; Tan, S.; Shutthanandan, V.; Ramana, C.V. Structure, surface/interface chemistry and optical properties of W-incorporated β-Ga2O3 films made by pulsed laser deposition. RSC Applied Interfaces 2024, 1, 1395–1409. https://doi.org/10.1039/d4lf00257a

[35] Cooke, J.; Sensale-Rodriguez, B.; Ghadbeigi, L. Methods for synthesizing β-Ga2O3 thin films beyond epitaxy. Journal of Physics: Photonics 2021, 3, 032005. https://doi.org/10.1088/2515-7647/ac0db5

[36] Li, X.; Niu, J.; Bai, L.; Jing, X.; Gao, D.; Deng, J.; Lu, F.; Wang, W. Preparation of β-Ga2O3/ε-Ga2O3 type II phase junctions by atmospheric pressure chemical vapor deposition. Ceramics International 2025, 51, 10395–10401. https://doi.org/10.1016/j.ceramint.2024.12.472

[37] Delpech, S.; Carrière, C.; Chmakoff, A.; Martinelli, L.; Rodrigues, D.; Cannes, C. Corrosion Mitigation in Molten Salt Environments. Materials (Basel) 2024, 17. https://doi.org/10.3390/ma17030581

[38] Faisal, N.H.; Rajendran, V.; Prathuru, A.; Hossain, M.; Muthukrishnan, R.; Balogun, Y.; Pancholi, K.; Hussain, T.; Lokachari, S.; Horri, B.A.; et al. Thermal spray coatings for molten salt facing structural parts and enabling opportunities for thermochemical cycle electrolysis. Engineering Reports 2024, 6, e12947. https://doi.org/10.1002/eng2.12947

[39] Dimitrocenko, L.; Strikis, G.; Polyakov, B.; Bikse, L.; Oras, S.; Butanovs, E. The Effect of a Nucleation Layer on Morphology and Grain Size in MOCVD-Grown β-Ga2O3 Thin Films on C-Plane Sapphire. Materials 2022, 15, 8362. https://doi.org/10.3390/ma15238362

[40] Wang, X.; Chen, Z.; Zhang, F.; Saito, K.; Tanaka, T.; Nishio, M.; Guo, Q. Temperature dependence of Raman scattering in β-(AlGa)2O3 thin films. AIP Advances 2016, 6. https://doi.org/10.1063/1.4940763

[41] Chen, Y.; Xia, X.; Liang, H.; Abbas, Q.; Liu, Y.; Du, G. Growth Pressure Controlled Nucleation Epitaxy of Pure Phase ε- and β-Ga2O3 Films on Al2O3 via Metal–Organic Chemical Vapor Deposition. Crystal Growth & Design 2018, 18, 1147–1154. https://doi.org/10.1021/acs.cgd.7b01576

[42] Usseinov, A.; Koishybayeva, Z.; Platonenko, A.; Pankratov, V.; Suchikova, Y.; Akilbekov, A.; Zdorovets, M.; Purans, J.; Popov, A.I. Vacancy Defects in Ga2O3: First-Principles Calculations of Electronic Structure. Materials 2021, 14, 7384. https://doi.org/10.3390/ma14237384

[43] Dong, L.; Jia, R.; Xin, B.; Peng, B.; Zhang, Y. Effects of oxygen vacancies on the structural and optical properties of β-Ga2O3. Scientific Reports 2017, 7, 40160. https://doi.org/10.1038/srep40160

[44] Milchev, A. Nucleation phenomena in electrochemical systems: thermodynamic concepts. ChemTexts 2016, 2, 2. https://doi.org/10.1007/s40828-015-0022-0

[45] Bosi, M.; Seravalli, L.; Mazzolini, P.; Mezzadri, F.; Fornari, R. Thermodynamic and Kinetic Effects on the Nucleation and Growth of ε/κ- or β-Ga2O3 by Metal–Organic Vapor Phase Epitaxy. Crystal Growth & Design 2021, 21, 6393–6401. https://doi.org/10.1021/acs.cgd.1c00863

[46] Xu, Y.; Zhang, C.; Cheng, Y.; Li, Z.; Cheng, Y.n.; Feng, Q.; Chen, D.; Zhang, J.; Hao, Y. Influence of Carrier Gases on the Quality of Epitaxial Corundum-Structured α-Ga2O3 Films Grown by Mist Chemical Vapor Deposition Method. Materials 2019, 12, 3670. https://doi.org/10.3390/ma12223670

[47] Wang, J.; Luo, T.-c.; He, Y.-c.; Wang, G. Chemical reaction-mass transport model of Ga2O3 grown by TEGa in MOCVD and an intelligent system. Journal of Crystal Growth 2023, 618, 127311. https://doi.org/10.1016/j.jcrysgro.2023.127311

[48] Karthika, S.; Radhakrishnan, T.K.; Kalaichelvi, P. A Review of Classical and Nonclassical Nucleation Theories. Crystal Growth & Design 2016, 16, 6663–6681. https://doi.org/10.1021/acs.cgd.6b00794

[49] Yu, H.Z.; Thompson, C.V. Grain growth and complex stress evolution during Volmer–Weber growth of polycrystalline thin films. Acta Materialia 2014, 67, 189–198. https://doi.org/10.1016/j.actamat.2013.12.031